01

# Effect of electric field on circular photovoltaic effect in topological superlattice

© P.V. Badikova, D.V. Zavyalov, E.S. Sivashova

Volgograd State Technical University,
400005 Volgograd, Russia
e-mail: polin.badicova@gmail.com

Received October 11, 2024
Revised October 11, 2024
Accepted October 11, 2024

The influence of a constant electric field on the circular photovoltaic effect in an anisotropic graphene superlattice at normal incidence is investigated. An expression for the current density in such a superlattice is obtained.

**Keywords:** graphene, superlattice, graphene-based superlattice, circular photovoltaic effect.

DOI: 10.61011/TP.2025.03.60845.310-24

## Introduction

Circular photovoltaic effect is one of the methods to study the kinetic properties of the material. It consists in generation of DC in the material when exposed to obliquely incident elliptically polarized electromagnet wave in the direction perpendicular to the project of wave vector on the specimen plane. The DC current value may indicate the properties of emission and the properties of the structure. The effect is directly to the presence of spin in the charge carriers and is better studied in the materials with a hamiltonian containing a summand linear by quasi-momentum module and explicitly taking into account the spin-orbit interaction (so called Rashba and Dresselhaus hamiltonians) [1–4]. [5] did the calculations with the help of the density functional theory and the Green's non-equilibrium function method to study the photovoltaic effect of a single-layer lateral heterojunction $WSe_2-MoS_2$ under vertical radiation.

Interaction between light with circular polarization and quantum materials strengthens in chiral spatial groups due to structural chirality. Paper [6] studies the tunable circular photoelectric responses in field transistors $2D$ Te with different chirality, including longitudinal circular photovoltaic effect induced by radial spin texture (polarization of spin and electron is parallel to the direction of the electron impulse), and circular thermovoltaic effect induced by chiral crystalline structure (spiral chains of Te atoms). Circular photovoltaic and photoelectric effects strongly depend on chirality of Te crystals, which makes $2D$ Te the material for development of optoelectronic devices depending on chirality. [7] developed the general theory of laminar circular photovoltaic effect in quasi-two-dimensional chiral bilayers which related to the appearance of polarization-dependent out-of-plane static dipole moment induced by circularly polarized light. The laminar circular photovoltaic effect was calculated in the twisted two-layer graphite, and it was found that it demonstrates the resonant peak, the frequency of which may be tuned from visible to infrared one as the twisting angle varies. Therefore, the laminar circular photovoltaic effect provides a promising path to frequency-sensitive detection of light with circular polarization, especially in the infrared range.

Circular photovoltaic effect is useful to study topological half-metals, since the tensor of circular photovoltaic effect quantizes well isolated topological degeneracy in strictly linear-dispersion band structures. [8,9] studied multiplicative half-metal Weyl band structures and it was found that the multiplicative structure reliably protects the quantization of circular photovoltaic effect even in case of non-linear dispersion. Besides, this effect may be used to identify the complex topology, differing the topological degeneracies of multiplicative topological half-metals on allegedly similar topological degeneracies by degree of degeneracy and total topological charge, for example, Dirac nodes.

Paper [10] studies the photovoltaic effects in centrosymmetric two-dimensional materials, two-layer graphene, folded as AA and AB [11], by applying external voltage on the gate to disturb the inversion symmetry. Using approximation of strong bond to describe electron states, injection coefficients were calculated for the circular photovoltaic effect for both materials with wavelengths from terahertz to visible range. It was shown that photovoltaic effects induced by gate voltage may be rather significant for the two-layer graphene folded as AB.

Article [12] presents the study of the photoelectric effect of double heterostructure graphene/$MoS_2$/Si, grown by method of fast chemical deposition from vapor phase. It was found that double transitions of graphene/$MoS_2$-Schottky transition and heterostructures $MoS_2$/Si play an important role in increased efficiency of the device. They made it possible to effectively generate, separate and collect more electron-hole pairs on a double interface of graphene/$MoS_2$/Si.

Paper [13] studied the photoresistance of cyclotron resonance in 2D electronic systems based on GaAs. Abnormally low sensitivity to helicity of the arriving circularly polarized terahertz radiation was found. It was found that this abnormality strongly depends on intensity.

Note that such effect is possible in the materials, for which spin-orbit interaction is not specific, in this case DC appears due to the transfer of the angular momentum of photon to free charge carriers, and the effect is due to not the spin orientation, but is purely orbital. Such materials include $d$-wave superconductors [14,15], graphene [16], phosphorene [17], silicene [18] and topological insulators [19], which have fundamental similarity: their low-energy fermionic excitations behave as massless Dirac particles, and not as fermions that are subordinate to a regular Schrödinger hamiltonian. Materials united by such properties were called „Dirac materials" [20,21].

Note that superlattices may be created on the basis of such materials, where the circular photovoltaic effect will be possible, but also the response nonlinearity structures related to features of the energy spectrum should also manifest themselves. One of the superlattices is a superlattice based on graphene (GSL). There are many methods of GSL representation [22–26]: use of electrostatic and magnetic barriers, alternation of graphene single- and bilayer, use of graphene nanoribbons, deposition of graphene on the substrate, which contains the periodically arranged layers of various dielectrics, and alternation of graphene layers at different angle of rotation relative to each other. Apart from theoretical modeling, GSL was implemented experimentally. [27] reports a new approach to making 2$D$ GSL, where the superlattice potential is modulated by the substrate with the periodically arranged nanoholes. Paper [28] studies the unique 2$D$ SL, produced as a result of the graphene deposition on the sub from metal nanoballs. Study of the electron transport in the graphene field transistor with a double gate placed on the folded twisted bilayer $WSe_2$ at the twisting angle $2.1^\circ$ is presented in [29]. The article presents the hysteresis characteristics of transfer and studies the heterogeneity of the charge with several local Dirac points as the electric shift field increases.

Moire patterns from 2D (2$D$) heterostructures of graphene assembled with the help of Van der Waals interactions, are studied in paper [30]. Such patterns arise in the two-layer superlattice of graphone (half-hydrogenated graphene)/graphene obtained as a result of direct single-sided hydrogenation of two-layer graphene on the substrate. Compared to source graphene, the two-layer superlattice has corrugated surface. These moire patterns are detected with atomic-force microscopy and additionally confirmed by the fast Fourier transform analysis. High mobility of charge carriers in the moire superlattice based on graphene and disturbance of the inversion symmetry by hexagonal boron nitride cause nonlinear conductance [31]. Nonlinear conductance strongly depends on the gate voltage and on the configuration of the layers in the structure, besides, the huge amplification is related to moire bands.

Apart from the classical superlattices, multiple heterostructures based on graphene were studied [32]. Paper [33] studies the segnetoelectric photoelectric effect that depends on the thickness of segnetoelectric layer, in the vertical multi-layer heterostructures of graphene/$\alpha$-$In_2Se_3$/graphene. It is shown that the photocurrent of short circuit is anti-parallel to segnetoelectric polarization and increases exponentially as thickness decreases. Photocurrent generation was studied in the tunnel structures of graphene/$h$-BN/graphene with localized defect states at illumination with light of middle IR range [34]. It was shown that the photocurrent in these devices is proportionate to the second derivative of the tunnel current by shift voltage, reaching the maximum when tunneled through the impurity level $h$-BN. It was found that the reason for photocurrent generation consists in changing the photon tunneling probability under radiation-induced heating of electrons in graphene layers.

Since in GLS non-linear effects arise at comparatively low field intensities, the study of the circular photovoltaic effect in such structures is of interest. This paper studies how the DC field directed along alternation of the layers impacts the circular photovoltaic effect in the anisotropic graphene superlattice. The analytical expression for current density was produced, and its dependence on various parameters of electric fields was studied.

## 1. Calculation of constant component in current density

The hamiltonian of the superlattice based on Dirac material with one-dimensional potential looks as follows [35]:

$$\upsilon_F \hat{p}_x \hat{\sigma}_x \psi + \left(V(x) + \alpha \hat{p}_y^2\right)\sigma_y \psi = \varepsilon \psi, \tag{1}$$

where $\alpha = 1/2m^*$, and spatial modulation profile $V(x)$ is set by Kronig–Penney model:

$$V(x) = \begin{cases} \Delta_1, & (s-1)d < x < a + (s-1)d, \\ \Delta_2, & a + (s-1)d < x < s. \end{cases} \tag{2}$$

Energy spectrum of the considered structure in the low energy approximation is as follows [35]:

$$\varepsilon(p) = \pm 2F\sqrt{\sin^2\left(\frac{p_x}{2}\right) + 1/4\,(p_y^2 + \Delta_{\text{eff}})^2}, \tag{3}$$

where $\Delta_{1,2} = \Delta_{1,2} d/\upsilon_{\text{F}}$ — band gap half-width,

$$\Delta_{\text{eff}} = \frac{\Delta_1 + n\Delta_2}{1+n},\ F = \frac{Q}{\operatorname{sh} Q},\ Q = n\,\frac{(\Delta_2 - \Delta_2)}{(1+n)^2},$$

$p_x = p_x/d$, $p_y^2 = \alpha p_y^2 d/\nu_{\text{F}}$, $n = b/a$, $a, b$ — width of well and barrier accordingly, $d = a + b$ — superlattice period (fig. 1). Different signs are related to valence band and conduction band. Transitions between the half-metal state and band insulator are due to parameter $\Delta$. When $\Delta$ is negative, a saddle point appears in the spectrum. Increase of $\Delta$ causes the situation when the saddle point and

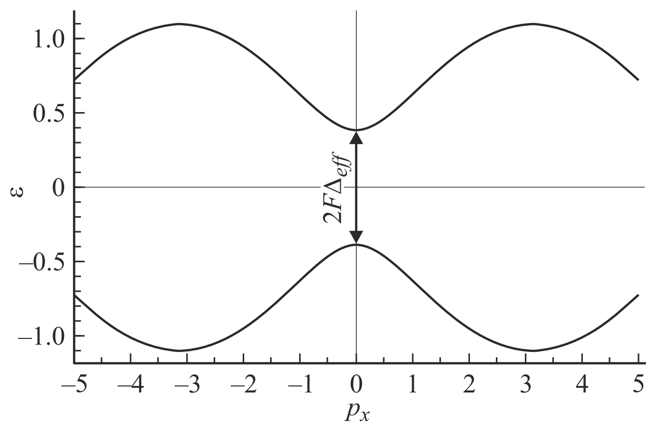


**Figure 1.** GSL band structure: $\Delta_1 = -5$, $\Delta_2 = 3.5$, $n = 1$, $p_y = 0$.

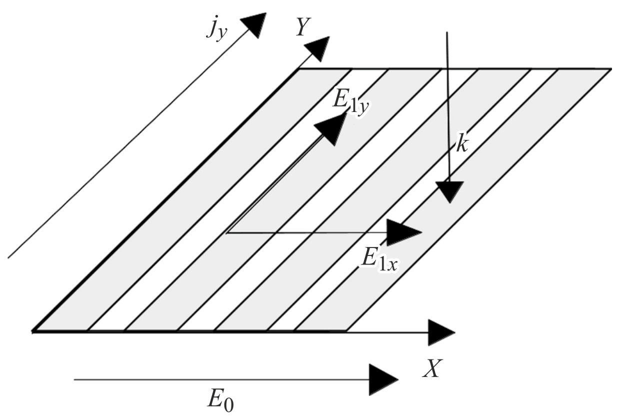


**Figure 2.** Problem geometry.

both Dirac points evolve into a single local minimum of the spectrum on transition (at $\Delta = 0$) to slot opening (at $\Delta > 0$). The superlattice considered in this paper is formed by alternation of bands of two Diract 2D-crystals with different values of parameter $\Delta$ ($\Delta_1$ and $\Delta_2$), parameters $\Delta_1$ and $\Delta_2$ determine the potential value in the area of the well and barrier.

We will consider the superlattice response to the action of DC and AC fields

$$\mathbf{E} = \big(E_{1x}\cos(\omega t) + E_0;\ E_{1y}\cos(\omega t + \varphi)\big),$$

where $E_0$ — module of DC field intensity, $E_{1x,y}, \omega$ — amplitude and frequency of AC field.

Density of current $jy$, flowing along axis $Y$ (fig. 2) is determined using formula

$$j_y = \langle e\Sigma_p v_y\, f(p,t)\rangle_t, \tag{4}$$

where $e$ — electron charge, $f(p,t)$ — non-equilibrium function of carrier distribution.

We will find the distribution function with the help of the classic Boltzmann equation

$$\frac{\partial f(p,t)}{\partial t} + eE\,\frac{\partial f(p,t)}{\partial p} = -\nu[f(p,t) - f_0(p)], \tag{5}$$

where $f_0(p)$ — equilibrium distribution function, $\nu$ — frequency of collisions.

The speed of electron movement along axis $y$ has the following appearance

$$v_y = \frac{\partial \varepsilon(p)}{\partial p_y} = \frac{F p_y(p_y^2 + \Delta_{\text{eff}})}{\sqrt{\sin^2(p_x/2) + 1/4(p_y^2 + \Delta_{\text{eff}})^2}}. \tag{6}$$

After speed decomposition by $p_y$ we obtain the following expression:

$$v_y \approx \frac{2F\Delta_{\text{eff}} p_y}{\sqrt{\sin^2(p_x/2) + \Delta_{\text{eff}}^2}}, \tag{7}$$

$$v_y'(x) = \frac{1}{\sqrt{\sin^2(p_x/2) + \Delta_{\text{eff}}^2}}. \tag{8}$$

Expand (8) in the composite Fourier series

$$v_y'(x) = \sum_{m=-\infty}^{+\infty} \hat{a}_m e^{imp_x}, \tag{9}$$

where

$$\hat{a}_m = \frac{1}{2\pi}\int_{-\pi}^{\pi} \frac{e^{imp_x}\,dp_x}{\sqrt{\sin^2(p_x/2) + \Delta_{\text{eff}}^2}}.$$

Solving equation (5) by method of characteristics, substituting it and (6) in (4), an expression for the current constant component is produced:

$$j_y = \frac{2e\nu}{(2\pi\hbar)^2}\Big\langle \int_{-\pi}^{\pi}\int_{-\infty}^{\infty}\int_{-\infty}^{t} e^{-\nu(t-t')} v_y(p_x; p_y) \times f_0\Big(p_x - \frac{e}{c}\big(A_x(t) - A_x(t')\big); p_y - \frac{e}{c}\big(A_y(t) - A_y(t')\big)\Big) d^2p\,dt'\Big\rangle_t. \tag{10}$$

Substitute variables

$$j_y = \frac{2e\nu}{(2\pi\hbar)^2}\Big\langle \int_{-\pi}^{\pi}\int_{-\infty}^{\infty}\int_{-\infty}^{t} e^{-\nu(t-t')} \times v_y\Big(p_x' + \frac{e}{c}\big(A_x(t) - A_x(t')\big); p_y' + \frac{e}{c}\big(A_y(t) - A_y(t')\big)\Big) f_0(p_x', p_y')\,d^2p'\,dt'\Big\rangle_t. \tag{11}$$

$$j_y = \frac{2e\nu}{(2\pi\hbar)^2}\frac{\hbar}{d}\sqrt{\frac{\nu_F\hbar}{\alpha d}}\left\langle \int_{-\pi}^{\pi}\int_{-\infty}^{\infty}\int_{-\infty}^{t} e^{-\nu(t-t')}\right.$$

$$\times\, \upsilon_y\left(p'_x - \frac{edE_{0x}}{\hbar\omega}\left(\sin(\omega t)-\sin(\omega t')\right) - \frac{edE_0}{\hbar}(t-t');\right.$$

$$\left. p'_y - \sqrt{\frac{\alpha d}{\nu_F\hbar}\frac{e}{\omega}}E_{0y}\left(\sin(\omega t+\varphi)-\sin(\omega t'+\varphi)\right)\right)$$

$$\left.\times f_0(p'_x, p'_y)d^2p'dt'\right\rangle_t. \quad (12)$$

Substitute (7) with account of decomposition of (10) in (12):

$$j_y = \frac{4e\nu F\Delta_{\text{eff}}}{(2\pi\hbar)^2}\frac{\hbar}{d}\sqrt{\frac{\nu_F\hbar}{\alpha d}}\left\langle \int_{-\pi}^{\pi}\int_{-\infty}^{\infty}\int_{-\infty}^{t} e^{-\nu(t-t')}\sum_{m=-\infty}^{+\infty}\hat{a}_m\right.$$

$$\times \exp\left[I\left(x - \frac{edE_{0x}}{\hbar\omega}\left(\sin(\omega t)-\sin(\omega t')\right) - \frac{edE_0}{\hbar}(t-t')\right)\right]$$

$$\times\left(y - \sqrt{\frac{\alpha d}{\nu_F\hbar}\frac{e}{\omega}}E_{0y}\left(\sin(\omega t+\varphi)-\sin(\omega t'+\varphi)\right)\right)$$

$$\left.\times f_0(x,y)dxdydt'\right\rangle_t. \quad (13)$$

After substitution of the $f_0$ distribution function and transition to new variables, we get

$$j_y = \frac{e\nu F\Delta_{\text{eff}}n_0}{I_0}\frac{\hbar}{d}\sqrt{\frac{\nu_F\hbar}{\alpha d}}\left\langle \int_{-\pi}^{\pi}\int_{-\infty}^{\infty}\int_{-\infty}^{t} e^{-\nu(t-t')}e^{\frac{-\varepsilon(x,y)}{kT}}\right.$$

$$\times \sum_{m=-\infty}^{+\infty}\hat{a}_m\exp[Ix]\exp\left[-i\alpha_{0x}\left(\sin(\omega t)-\sin(\omega t')\right)\right]$$

$$\left.\times\exp\left(y-\beta_{0y}\left(\sin(\omega t+\varphi)-\sin(\omega t'+\varphi)\right)\right)dxdydt'\right\rangle_t, \quad (14)$$

where

$$p'_x = x,\ p'_y = y,\ \alpha_{0x} = \frac{medE_{0x}}{\hbar\omega},\ \alpha_0 = \frac{medE_0}{\hbar},$$

$$\beta_{0y} = \sqrt{\frac{\alpha d}{\nu_F\hbar}\frac{e}{\omega}}E_{0y},\ I_0 = \int_{-\infty}^{\infty}\int_{-\pi}^{\pi}e^{\frac{-\varepsilon(x,y)}{kT}}dxdy.$$

Go to new variables: $t-t'=\tau$, $\omega t = k$ and using the fact that

$$e^{\pm iz\sin(t)} = \sum_{l=-\infty}^{\infty}J_l(z)e^{\pm ilt},$$

where $J_l(z)$ — Bessel function, we get

$$j_y = \frac{e\nu F\Delta_{\text{eff}}n_0}{I_0}\frac{\hbar}{d}\sqrt{\frac{\nu_F\hbar}{\alpha d}}\frac{1}{2\pi\omega}\int_{-\pi}^{\pi}\int_{-\infty}^{\infty}\int_{0}^{\infty}\int_{-\pi}^{\pi}e^{-\nu(\tau)}e^{\frac{-\varepsilon(x,y)}{kT}}$$

$$\times\sum_{m=-\infty}^{+\infty}\hat{a}_m e^{imx}e^{-\alpha_0\tau}\sum_{l=-\infty}^{\infty}J_l(\alpha_{0x})e^{-ilk}\sum_{z=-\infty}^{\infty}J_z(\alpha_{0x})e^{iz(k-\omega\tau)}$$

$$\times\left(y-\beta_{0y}\left(\sin(k+\varphi)-\sin(k-\omega\tau+\varphi)\right)\right)dkd\tau dxdy. \quad (15)$$

After integration by $k$ and $\tau$ expression (15) will look as follows

$$j_y = \frac{e\nu F\Delta_{\text{eff}}n_0}{I_0}\frac{\hbar}{d}\sqrt{\frac{\nu_F\hbar}{\alpha d}}\frac{1}{2\pi\omega}\int_{-\pi}^{\pi}\int_{-\infty}^{\infty}e^{\frac{-\varepsilon(x,y)}{kT}}$$

$$\times\sum_{m=-\infty}^{+\infty}\hat{a}_m e^{imx}\sum_{l=-\infty}^{\infty}\sum_{z=-\infty}^{\infty}J_z(\alpha_{0x})J_l(\alpha_{0x})\times$$

$$\frac{\begin{array}{c}-ie^{-i(\varphi+\pi(l-z)))}(e^{2i\pi(l-z)}-1)\beta_{oy}\omega\big(-e^{2i\varphi}(\alpha_0-i\nu\\ +\omega(z-1))(l+1-z)-(l-1-z)(\alpha_0-i\nu+\omega(z+1))\big)\end{array}}{\begin{array}{c}2(\alpha_0-i\nu+\omega(z-1))(l+1-z)(l-1-z)\\ \times(\alpha_0-i\nu+\omega(z+1))(\alpha_0-i\nu+\omega z)\end{array}}dxdy. \quad (16)$$

Break expression (16) into two fractions

$$j_y = \frac{e\nu F\Delta_{\text{eff}}n_0}{I_0}\frac{\hbar}{d}\sqrt{\frac{\nu_F\hbar}{\alpha d}}\frac{1}{2\pi\omega}\int_{-\pi}^{\pi}\int_{-\infty}^{\infty}e^{\frac{-\varepsilon(x,y)}{kT}}$$

$$\times\sum_{m=-\infty}^{+\infty}\hat{a}_m e^{imx}\sum_{l=-\infty}^{\infty}\sum_{z=-\infty}^{\infty}J_l(\alpha_{0x})\left(\frac{-\beta_{0y}\omega}{2}\right)\times$$

$$\left.\frac{\begin{array}{c}-ie^{-i(\varphi+\pi(l-z))}(e^{2i\pi(l-z)}-1)J_z(\alpha_{0x})(l-1-z)\\ \times(\alpha_0-i\nu+\omega(z+1))\end{array}}{\begin{array}{c}(\alpha_0-i\nu+\omega(z-1))(l+1-z)(l-1-z)\\ \times(\alpha_0-i\nu+\omega(z+1))(\alpha_0-i\nu+\omega z)\end{array}}\right\}dxdy. \quad (17)$$

Considering that

$$\lim_{x\to\mp 1}\frac{(e^{2i\pi(x)}-1)}{x\pm 1} = 2i\pi,$$

in the first fraction we substitute $z = l-1$, and in the second $z = l+1$;

$$j_y = \frac{e\tilde{\nu}F\Delta_{\text{eff}}n_0}{I_0}\frac{\hbar}{d}\sqrt{\frac{\nu_F\hbar}{\alpha d}}\int_{-\pi}^{\pi}\int_{-\infty}^{\infty}e^{\frac{-\varepsilon(x,y)}{kT}}\sum_{m=-\infty}^{+\infty}\hat{a}_m e^{imx}$$

$$\times\sum_{l=-\infty}^{\infty}J_1(\alpha_{0x})(-\beta|0y)\left\{\frac{e^{i(\varphi-\pi)}J_{l-1}(\alpha_{0x})}{(\tilde{\alpha}_0-i\tilde{\nu}+(l-1))(\tilde{\alpha}_0-i\tilde{\nu}+l)}\right.$$

$$\left.\times\frac{+e^{-i(\varphi-\pi)}J_{l+1}(\alpha_{0x})}{(\tilde{\alpha}_0-i\tilde{\nu}+(l+1))(\tilde{\alpha}_0-i\tilde{\nu}+l)}\right\}dxdy. \quad (18)$$

where $\tilde{\nu} = \nu/\omega$, $\tilde{\alpha}_0 = \alpha_0/\omega$.

Since series by $l$ varies from $-\infty$ to $+\infty$, in the first fraction we substitute $l \to l+1$ and $e^{\pm i\pi} = -1$

$$j_y = \frac{e\tilde{\nu}F\Delta_{\text{eff}}n_0}{I_0}\frac{\hbar}{d}\sqrt{\frac{v_F\hbar}{\alpha d}}\int_{-\pi}^{\pi}\int_{-\infty}^{\infty}e^{\frac{-\varepsilon(x,y)}{kT}}\sum_{m=-\infty}^{+\infty}\hat{a}_m e^{imx}$$
$$\times\sum_{l=-\infty}^{\infty}\beta_{0y}\left\{\frac{e^{i\varphi}J_l J_{l+1}(\alpha_{0x})}{(\tilde{\alpha}_0 - i\tilde{\nu} + l)(\tilde{\alpha}_0 - i\tilde{\nu} + (l+1))}\right.$$
$$\times\left.\frac{+e^{-i\varphi}J_l J_{l+1}(\alpha_{0x})}{(\tilde{\alpha}_0 - i\tilde{\nu} + (l+1))(\tilde{\alpha}_0 - i\tilde{\nu} + l)}\right\}dxdy. \quad (19)$$

The final expression for current density is written as

$$j_y = j_0\sum_{m=-\infty}^{+\infty}\hat{a}_m C_m\sum_{l=-\infty}^{\infty}\frac{\beta_{0y}J_l J_{l+1}(\alpha_{0x})\{e^{i\varphi} + e^{-i\varphi}\}}{(\tilde{\alpha}_0 - i\tilde{\nu} + l)(\tilde{\alpha}_0 - i\tilde{\nu} + (l+1))}, \quad (20)$$

where

$$C_m = \frac{1}{I_0}\int_{-\pi}^{\pi}\int_{-\infty}^{\infty}e^{\frac{-\varepsilon(x,y)}{kT}}e^{imx},\quad j_0 = \frac{\hbar e\tilde{\nu}F\Delta_{\text{eff}}n_0}{d}\sqrt{\frac{v_F\hbar}{\alpha d}}.$$

## 2. Numerical analysis of current density expression

Numerical studies were carried out with Wolfram Mathematica software based on Wolfram programming language. It focuses on symbolic computations, functional programming and rule-based programming and may use random structures and data.

Fig. 3 shows the dependence of constant component in current density on intensity of DC and amplitude of AC electric field applied along axis $X$, at $\beta_{0y} = 1.0$ and $\varphi = \pi/4$. Dependence of current on amplitude of the field of the wave polarized along the superlattice axis is of oscillating nature. The highest amplitude of oscillations is achieved in the area of weak fields. One dimensionless unit $\alpha, \beta$ corresponds to 65.8 V/cm, one unit $\Delta_{1,2}$ is equal to 0.0329 eV. Fig. 4 shows the dependence of the DC current density along axis $Y$ on amplitude of AC electric field of the wave polarized along axis $X$, at several values of DC electric field intensity. Fig. 5 shows the dependence of the DC current density along axis $Y$ on the intensity of DC electric field at several values of amplitude of the AC field polarized along axis $X$.

Note that paper [36] studied the circular photovoltaic effect in a related structure. Dependence of current density in the direction perpendicular to the axis of superlattice on the DC field intensity was of somewhat other nature.

$$j_y = j_0\beta_{0y}\sum_{l=-\infty}^{\infty}J_l(\alpha_{0x})\big(J_{l+1}(\alpha_{0x}) - J_{l-1}(\alpha_{0x})\big)$$
$$\times\frac{(\tilde{\alpha}_0^2 - l^2 + \tilde{\nu}^2)}{\big((\tilde{\alpha}_0 - l)^2 + \tilde{\nu}^2\big)\big((\tilde{\alpha}_0 + l)^2 + \tilde{\nu}^2\big)}\cos\varphi. \quad (21)$$

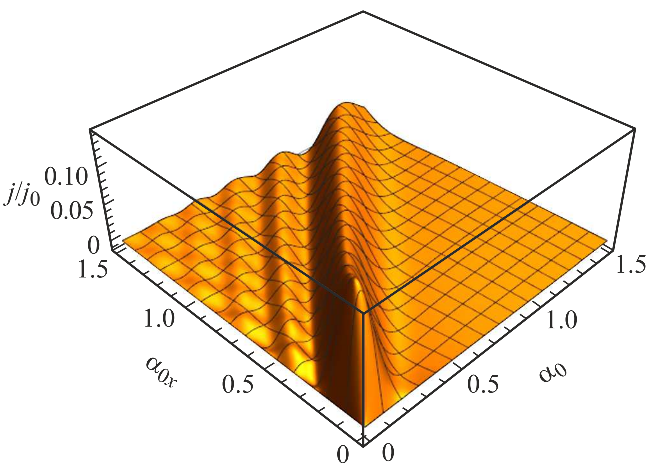


**Figure 3.** Dependence of current density on intensity of DC and amplitude of AC electric field applied along axis $X$ at $\beta_{0y} = 1.0$, $\varphi = \pi/4$, $\Delta_1 = -5$, $\Delta_2 = 2$.

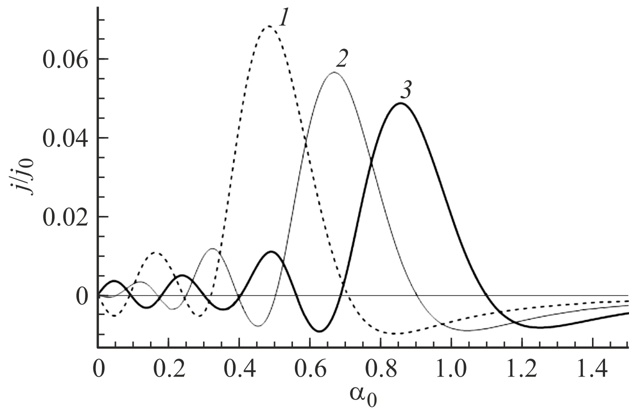


**Figure 4.** Dependence of current density on intensity of DC field applied along axis $X$ at fixed values: $\Delta_1 = -5$, $\Delta_2 = 2$, $\beta_{0y} = 1.0$, $\varphi = \pi/4$; $\alpha_{0x}$: *1* — 0.6; *2* — 0.8; *3* — 1.0.

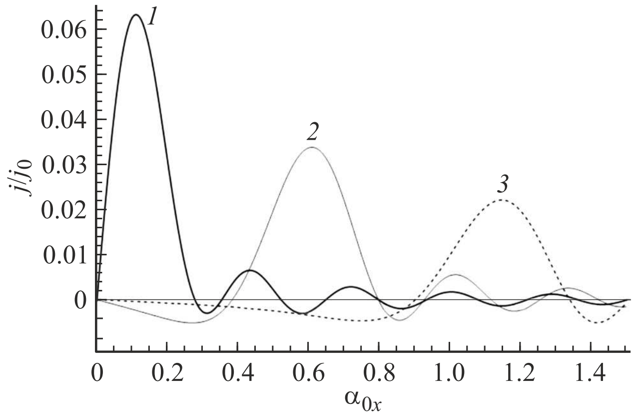


**Figure 5.** Dependence of current density on amplitude of AC field applied along axis $X$ at fixed values: $\Delta_1 = -5$, $\Delta_2 = 2$, $\beta_{0y} = 0.5$, $\varphi = \pi/4$; $\alpha_0$: *1* — 0.05; *2* — 0.5; *3* — 1.0.

Expression (21) has the structure specific for resonance, when the energy collected by electron at the distance equal to the superlattice period is numerically equal to the integer number of light quantum energies. Curves presented in fig. 5 do not show the second order breaks specific for the resonance. Expression (20) finds no resonant dependences. Such difference is due to the exceeded limits of quasi-classical approximation applicability in paper [36] when building the dependence of DC current density in the transverse direction on the DC field intensity.

Therefore, the impact of DC field was studied on the circular photovoltaic effect in the anisotropic graphene superlattice at normal incidence. An expression is produced for current density in such superlattice. Non-additivity of the graphene-based superlattice energy spectrum causes mutual dependence of the charge carrier movements in the directions perpendicular to each other, which, in particular, is the reason for appearance of the rectification current impact in such structure in the direction perpendicular to the drift field, under the action of the incident elliptically polarized wave incident on the surface. Besides, the current density in the transverse direction is approximately an order below the current density in the direction of the superlattice axis. Dependence of the current density on the intensity of the applied field has a non-monotonic nature. The nature of this dependence is similar to the nature of Stark resonance, known in the quantum semiconductor superlattices.

The above assumptions will be fair for the following parameters of the material: $T = 70\,\mathrm{K}$, $d = 2 \cdot 10^{-6}\,\mathrm{cm}$, $v_\mathrm{F} = 10^8\,\mathrm{cm/s}$.

### Conflict of interest

The authors declare that they have no conflict of interest.

## References


[1] V.I. Konchenkov, A.A. Myachkova, D.V. Zav’yalov. J. Phys.: Conf. Ser., **1697**, 012205 (2020). DOI: 10.1088/1742-6596/1697/1/012205
[2] S.A. Tarasenko. Phys. Rev. B, **83**, 035313 (2011). https://doi.org/10.1103/PhysRevB.83.035313
[3] G.V. Budkin, S.A. Tarasenko. Phys. Rev. B, **105**, L161301 (2022). https://doi.org/10.1103/PhysRevB.105.L161301
[4] P. Olbrich, S.A. Tarasenko, C. Reitmaier. Phys. Rev. B, **79**, 121302 (2009). https://doi.org/10.1103/PhysRevB.79.121302
[5] W.-M. Luo, Z.-G. Shao, X.-F. Qin, M. Yang. Physica E: Low-dimensional Systems and Nanostructures, **115**, 113714 (2020). https://doi.org/10.1016/j.physe.2019.113714
[6] C. Niu, S. Huang, N. Ghosh, P. Tan, M. Wang, W. Wu, X. Xu, P.D. Ye. Nano Lett., **23** (8), 3599 (2023). https://doi.org/10.1021/acs.nanolett.3c00780
[7] Y. Gao, Y. Zhang, D. Xiao. Phys. Rev. Lett., **124**, 077401 (2020). https://doi.org/10.1103/PhysRevLett.124.077401
[8] A. Pal, D. Varjas, A.M. Cook. ArXiv, 2023. https://doi.org/10.48550/arXiv.2312.03159
[9] A. Pal, J.H. Winter, A.M. Cook. Phys. Rev. B, **109**, 035147 (2024). https://doi.org/10.1103/PhysRevB.109.035147
[10] Z. Zheng, K. Chang, J.L. Cheng. Phys. Rev. B, **108**, 235401 (2023). https://doi.org/10.1103/PhysRevB.108.235401
[11] J. Nilsson, A.H. Castro Neto, F. Guinea, N.M.R. Peres. Phys. Rev. B, **78** (4), 045405 (2008). https://doi.org/10.1103/PhysRevB.78.045405
[12] W. Shi, X. Ma. Coatings, **8**, 2 (2018). https://doi.org/10.3390/ coatings8010002
[13] E. Mönch, S. Schweiss, I. Yahniuk, M.L. Savchenko, I.A. Dmitriev, A. Shuvaev, A. Pimenov, D. Schuh, D. Bougeard, S.D. Ganichev. Phys. Rev. Res., **6**, 023106 (2024). https://doi.org/10.1103/PhysRevResearch.6.023106
[14] Kazumi Maki. AIP Conf. Proc. **438** (1), 83 (1998). https://doi.org/10.1063/1.56343
[15] B. Cheng, D. Cheng, K. Lee, L. Luo, Z. Chen, Y. Lee, B.Y. Wang, M. Mootz, I.E. Perakis, Zhi-Xun Shen, H.Y. Hwang, W. Jigang. Nat. Mater., **23**, 775 (2024). https://doi.org/10.1038/s41563-023-01766-z
[16] K.S. Novoselov, A.K. Geim, S.V. Morozov, D. Jiang, Y. Zhang, S.V. Dubonos, I.V. Grigorieva, A.A. Firsov. Science, **306** (5696), 666 (2004). DOI: 10.1126/science.1102896
[17] Y. Kaddar, W. Zhang, H. Enriquez, Y.J. Dappe, A. Bendounan, G. Dujardin, O. Mounkachi, Abdallah El kenz, A. Benyoussef, A. Kara, H. Oughaddou. Adv. Functional Mater., **33** (21), 2213664 (2023). https://doi.org/10.1002/adfm.202213664
[18] H. Oughaddou. Silicene, a Promising New 2*D* Mater., **90** (1), 46 (2015). https://doi.org/10.1016/j.progsurf.2014.12.003
[19] J. Moore. Nature, **464**, 194 (2010). https://doi.org/10.1038/ nature08916
[20] J. Cayssol. Comp. Rendus Phys., **14** (9–10), 760 (2013). https://doi.org/10.1016/j.crhy.2013.09.012
[21] T.O. Wehling, A.M. Black-Schaffer, A.V. Balatsky. Adv. Phys., **63** (1), 1 (2014). https://doi.org/10.1080/00018732. 2014.927109
[22] S.C. Chen, R. Kraft, R. Danneau, K. Richter, M.-H. Liu. Commun. Phys., **3**, 71 (2020). https://doi.org/10.1038/s42005-020-0335-1
[23] H. Lv, Y. Yao, M. Yuan, G. Chen, Y. Wang, L. Rao, S. Li, U.I. Kara, R.L. Dupont, C. Zhang, B. Chen, B. Liu, X. Zhou, R. Wu, S. Adera, R. Che, X. Zhang, X. Wang. Nat. Commun., **15**, 1295 (2024). https://doi.org/10.1038/s41467-024-45503-9
[24] S.A.A. Ghorashi, J. Cano. Phys. Rev. B, **107**, 195423 (2023). https://doi.org/10.1103/PhysRevB.107.195423
[25] M. Pudlak, R.G. Nazmitdinov. Phys. Rev. B, **109**, 205402 (2024). https://doi.org/10.1103/PhysRevB.109.205402
[26] B. Wei, H. Ying, J. Chen, Q. Zang, J. Dong, H. Zhang, Y. Liu, C. Liu. Nanomaterials, **14** (12), 1019 (2024). https://doi.org/10.3390/nano14121019
[27] C. Forsythe, X. Zhou, K. Watanabe, T. Taniguchi, A. Pasupathy, P. Moon, M. Koshino, P. Kim, C.R. Dean. Nat. Nanotechnol., **13**, 566 (2018). https://doi.org/10.1038/s41565-018-0138-7
[28] Y. Zhang, Y. Kim, M.J. Gilbert, N. Mason. npj 2*D* Mater. Appl., **2**, 31 (2018). https://doi.org/10.1038/s41699-018-0076-0
[29] S. Sett, R. Debnath, A. Singha, S. Mandal, J.K.M. Bhakar, K. Watanabe, T. Taniguchi, V. Raghunathan, G. Sheet, M. Jain, A. Ghosh. ArXiv, 2024. https://doi.org/10.48550/ arXiv.2405.18024
[30] H. Li, R. Papadakis, T. Hussain, A. Karton, J. Liu. Nano Res., **13**, 1060 (2020). https://doi.org/10.1007/s12274-020-2744-6
[31] P. He, G.K.W. Koon, H. Isobe, J.Y. Tan, J. Hu, A.H. Castro Neto, L. Fu, H. Yang. Nat. Nanotechnol., **17**, 378 (2022). https://doi.org/10.1038/s41565-021-01060-6

[32] C. Dean, A.F. Young, L. Wang, I. Meric, G.-H. Lee, K. Watanabe, T. Taniguchi, K. Shepard, P. Kim, J. Hone. Solid State Commun., **152** (15), 1275 (2012). https://doi.org/10.1016/j.ssc.2012.04.021
[33] S.M. Nahid, S.W. Nam, A.M. van der Zande. ACS Nano, **18** (22), 14198 (2024). https://doi.org/10.1021/acsnano. 3c11558
[34] D.A. Mylnikov, M.A. Kashchenko, K.N. Kapralov, D.A. Ghazaryan, E.E. Vdovin, S.V. Morozov, K.S. Novoselov, D.A. Bandurin, A.I. Chernov, D.A. Svintsov. 2*D* Mater. Appl., **8**, 34 (2024). https://doi.org/10.1038/s41699-024-00470-z
[35] E.I. Kukhar, S.V. Kryuchkov. Superlattices and Microstructures, **133**, 106183 (2019). https://doi.org/10.1016/ j.spmi.2019.106183
[36] D.V. Zavyalov, V.I. Konchenkov, S.V. Kryuchkov. FTP (in Russian), **46** (1), 113 (2012).

*Translated by M.Verenikina*